

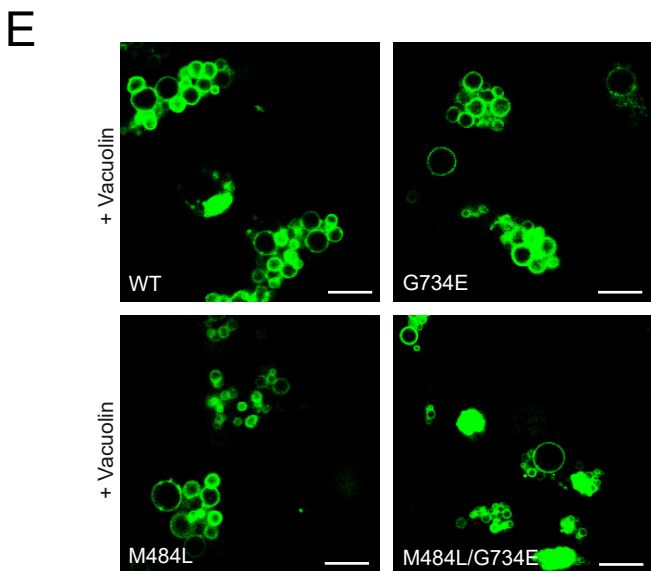
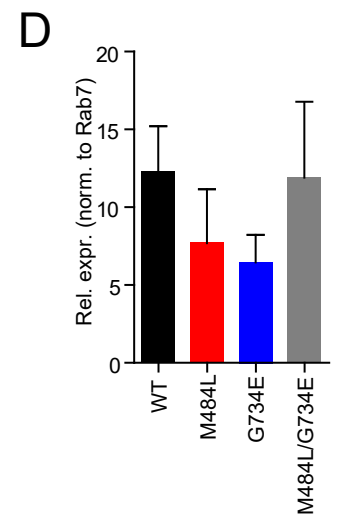
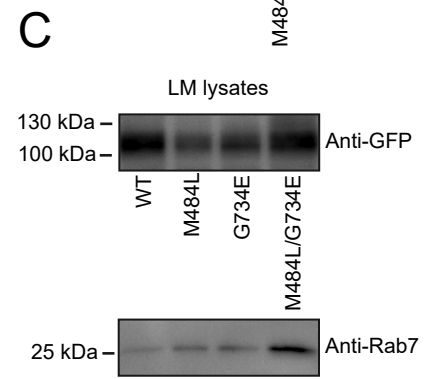
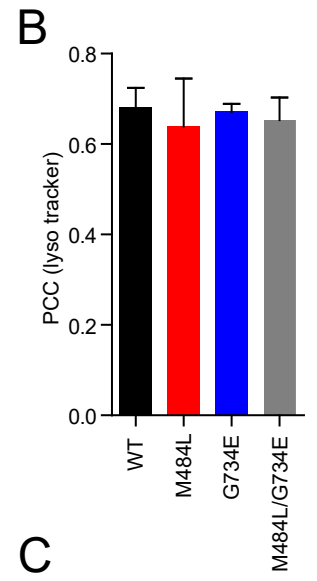
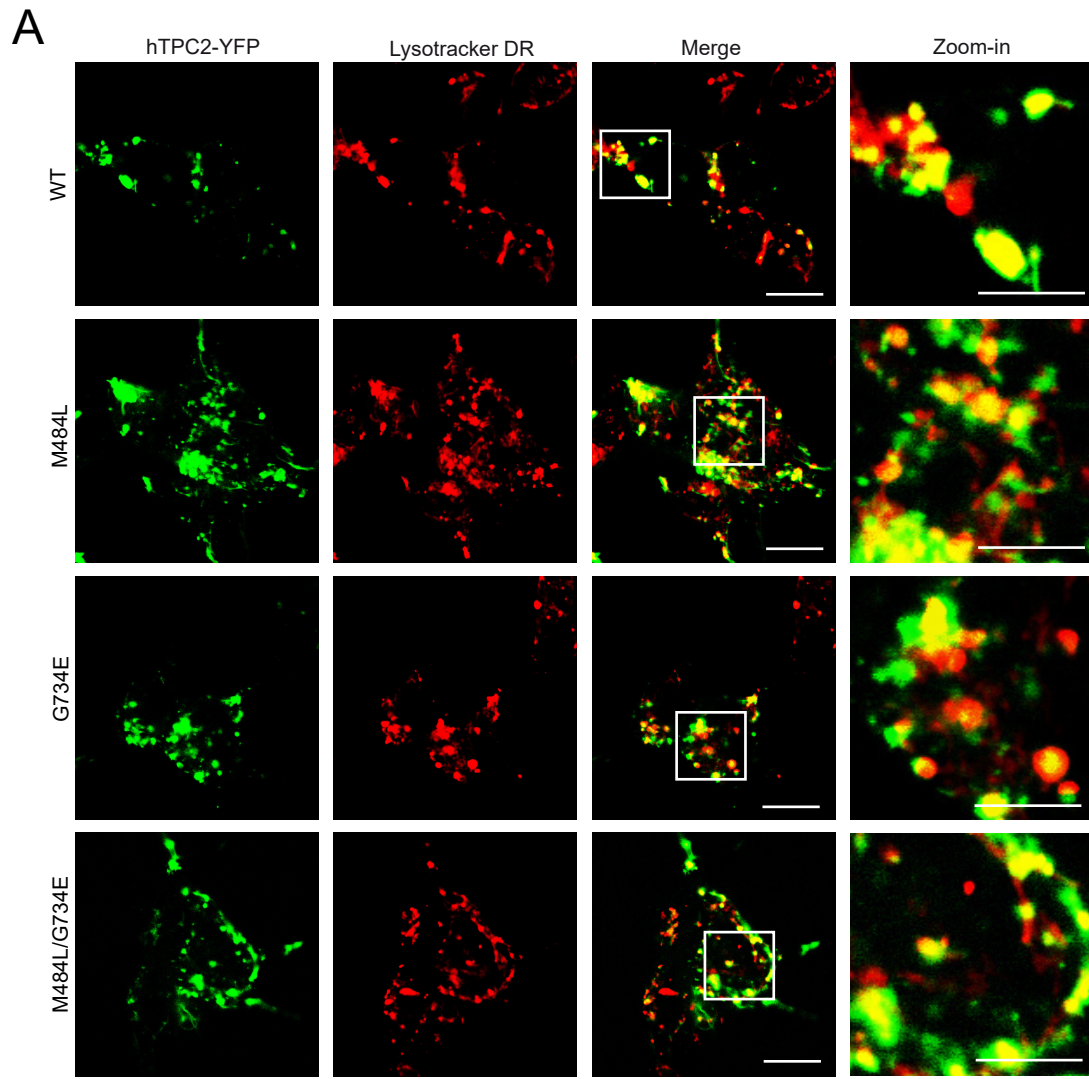
Chao et al.

Supporting information

TPC2 polymorphisms associated with a hair pigmentation phenotype in humans result in gain of channel function by independent mechanisms.

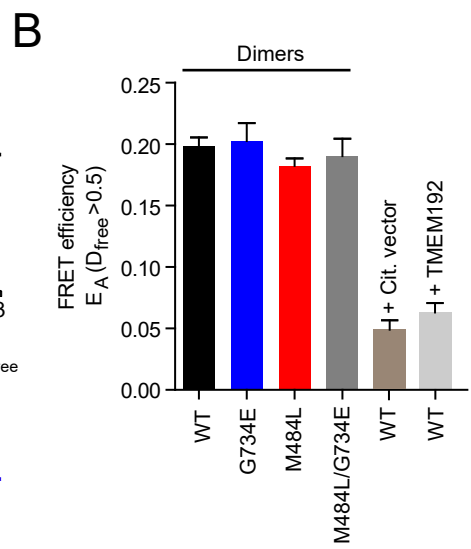
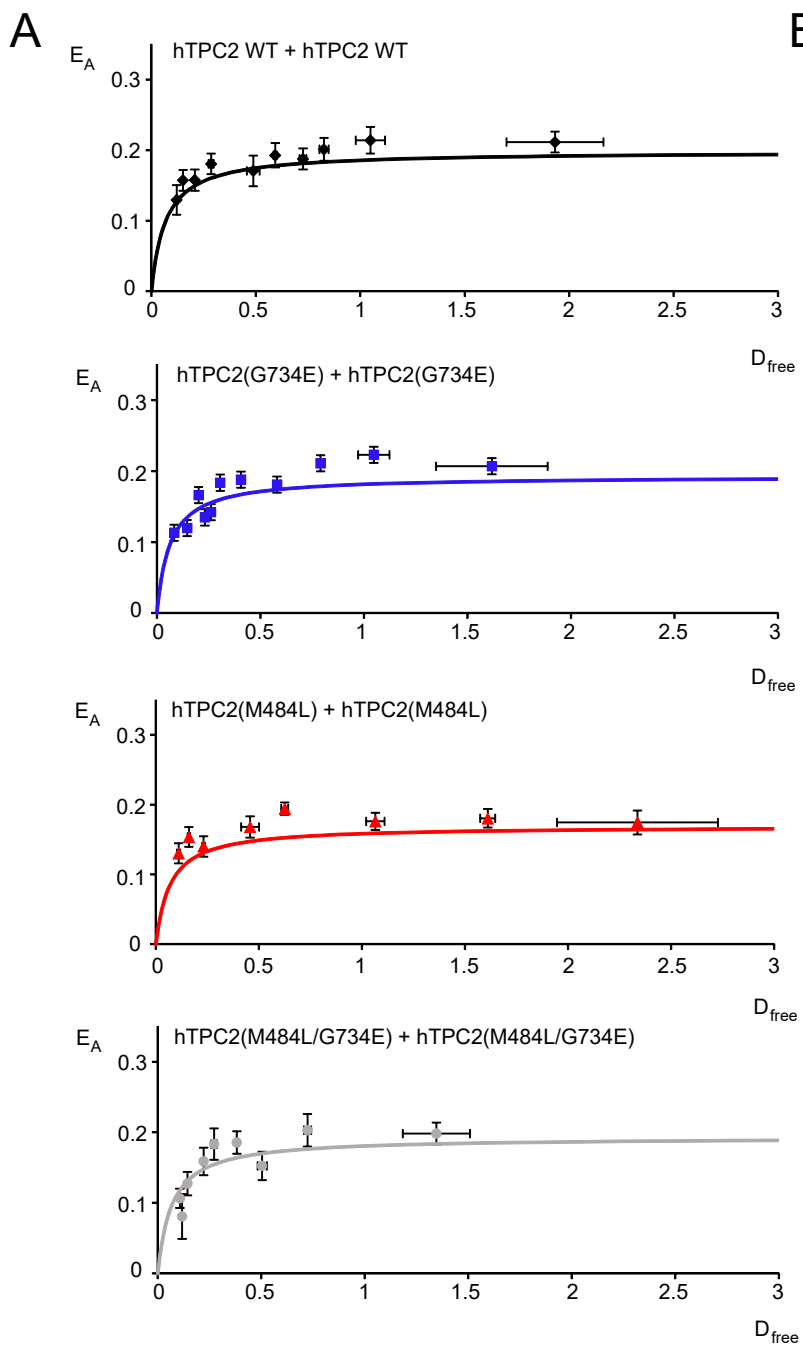
Yu-Kai Chao¹, Verena Schludi¹, Cheng-Chang Chen¹, Elisabeth Butz¹, O.N. Phuong Nguyen¹, Martin Müller¹, Jens Krüger², Claudia Kammerbauer³, Manu Ben-Johny⁴, Angelika Vollmar¹, Carola Berking³, Martin Biel¹, Christian Wahl-Schott¹, and Christian Grimm¹

¹Department of Pharmacy - Center for Drug Research and Center for Integrated Protein Science Munich (CIPSM), Ludwig-Maximilians-Universität München, Germany; ²High-Performance and Cloud Computing Group, Zentrum für Datenverarbeitung, Universität Tübingen, Germany; ³Department of Dermatology, Medical Faculty, Ludwig-Maximilians-Universität München, Germany; ⁴Calcium Signals Laboratory, Department of Biomedical Engineering, The Johns Hopkins University School of Medicine, Baltimore, Maryland, USA.



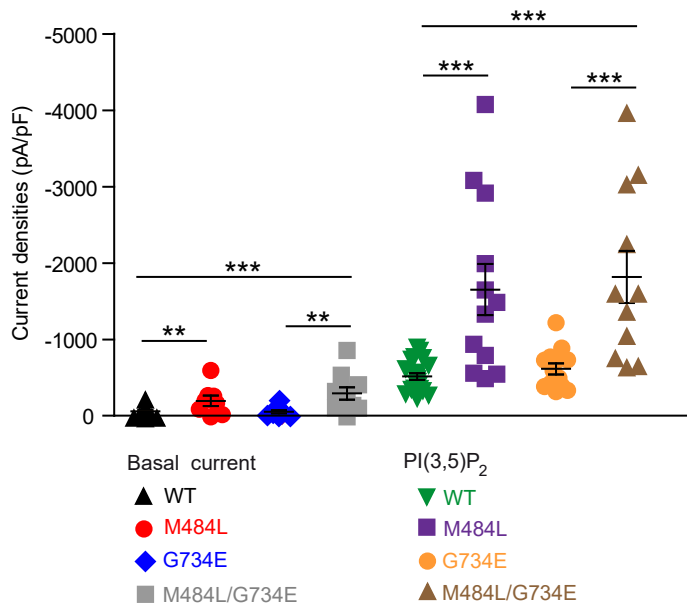
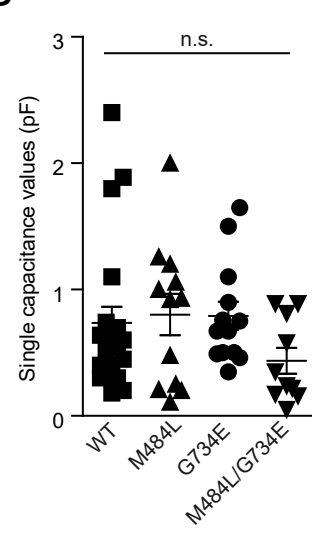
SI Figure 1

Human TPC2 WT and polymorphic variants: expression, subcellular distribution and vacuolin effect. (A) Shown are representative laser scanning images of hTPC2 WT and the polymorphic variants hTPC2(G734E), hTPC2(M484L), and hTPC2(M484L/G734E), all C-terminally fused to YFP and overexpressed in HEK293 cells using TurboFect. All isoforms showed a punctuated pattern and colocalized with LysoTracker DR (deep red). Scale bars = 10 μm (zoom-in images: scale bars = 5 μm). (B) PCC (Pearson correlation coefficients) calculated from images as shown in A using ImageJ software and the JACoP colocalization plugin (images were taken from $n = 3$ independent experiments). (C-D) Depicted in C are representative western blot data showing specific bands for hTPC2 WT and the polymorphic variants hTPC2(G734E), hTPC2(M484L), and hTPC2(M484L/G734E) fused to YFP, respectively, and detected with an anti-GFP antibody in lysosomal membranes (LM). LM were purified from whole cell lysates. The bands recognized with anti-Rab7 antibody were used as reference for the lysosomal preparations. Shown in D is the quantification of the data presented in C ($n = 3$ independent experiments) using Image Lab Software. All variants showed no significant differences in their relative expression levels. (E) The effect of vacuolin on all isoforms was comparable. Shown are representative laser scanning images of the respective variants overexpressed in HEK293 cells. Cells were treated for 4 hours with 1 μM vacuolin. Scale bars = 10 μm .



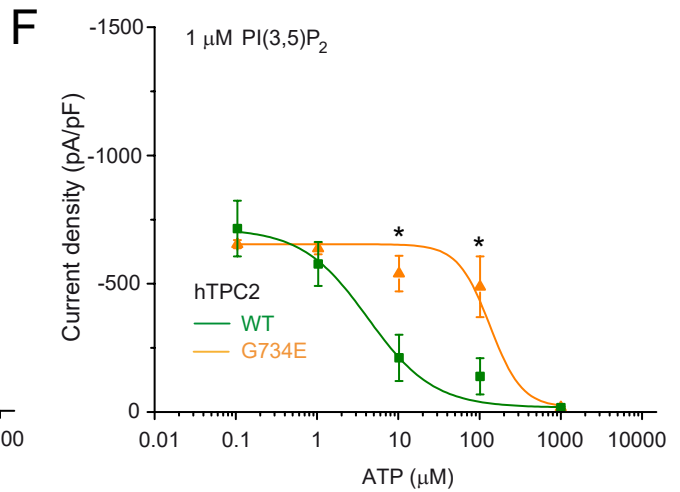
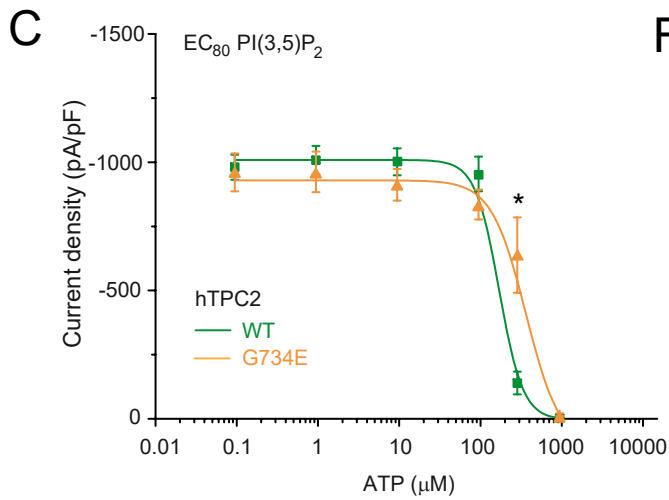
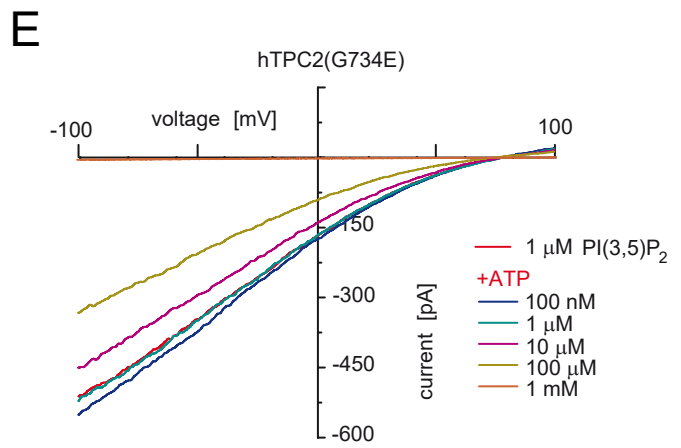
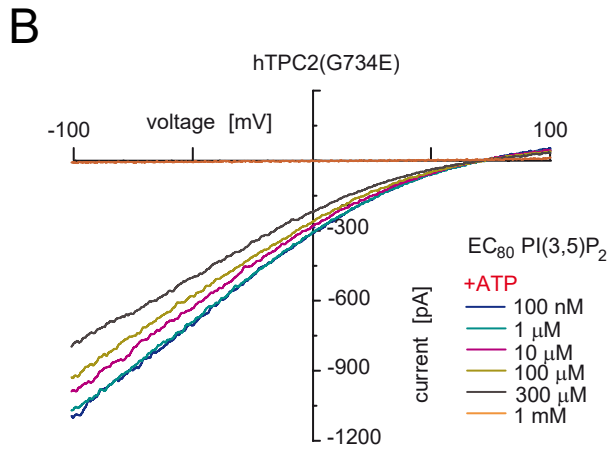
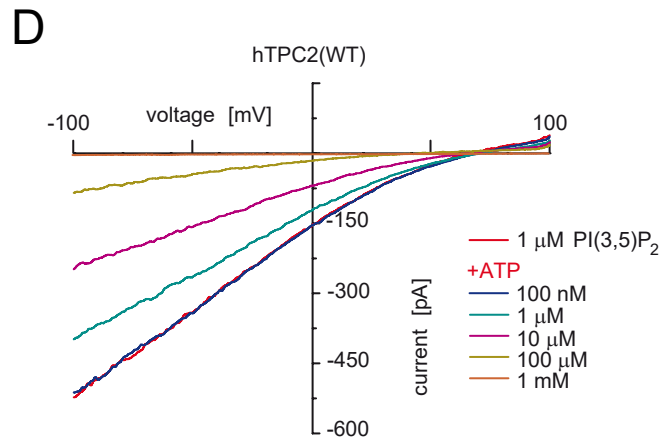
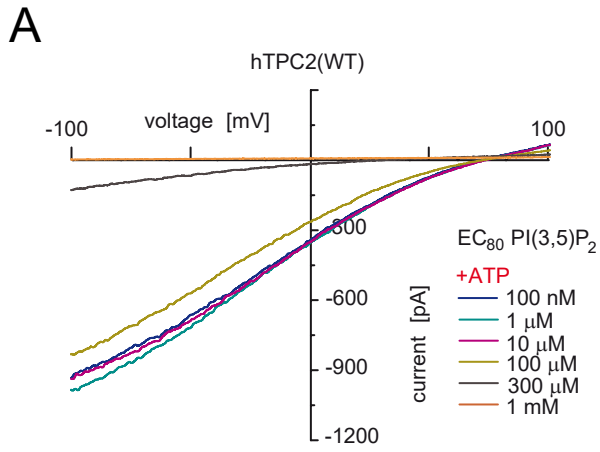
SI Figure 2

FRET experiments to assess TPC2 WT and polymorphic variant dimerization. (A) Shown are the respective FRET efficiencies (E_A) for binned groups of HEK293 cells overexpressing hTPC2 WT or the polymorphic variants hTPC2(G734E), hTPC2(M484L), or hTPC2(M484L/G734E), N-terminally fused to Citrine or Cerulean, respectively, plotted versus D_{free} , forming a binding curve. As negative control the lysosomal transmembrane protein hTMEM192 C-terminally fused to Cerulean was co-transfected with Citrine-hTPC2 WT. As a second negative control co-transfection of Cerulean-hTPC2 WT with empty Citrine-vector was used. (B) Statistical summary of data as shown in A using $D_{free} > 0.5$ as cutoff. In all statistical analyses mean values of at least 3 independent experiments ($n = 10-15$ cells each) are shown, each. To test for statistical significance one-way ANOVA test followed by Tukey's post-test was applied. No significant differences were found between the TPC2 variants.

A**B**

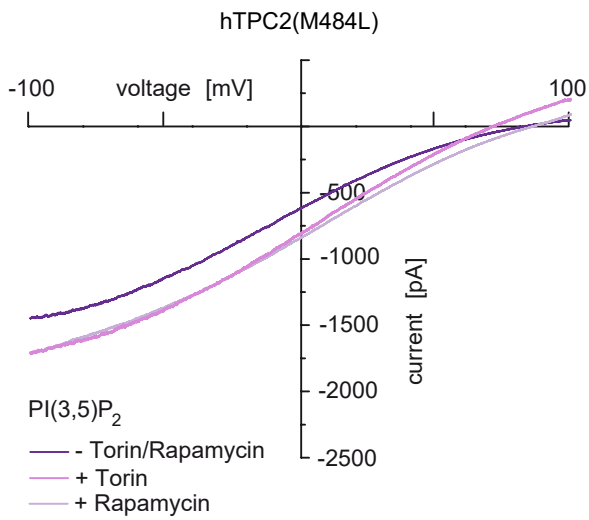
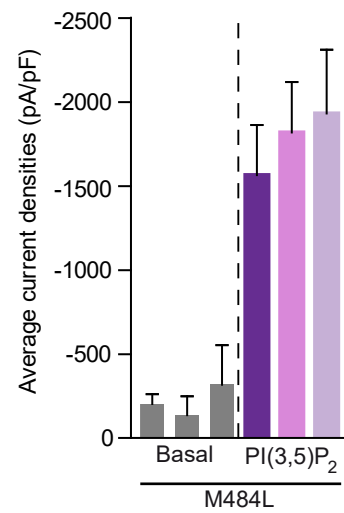
SI Figure 3

Effect of PI(3,5)P₂ on endolysosomal vesicles expressing either human TPC2 WT or polymorphic variants. (A) Single values of current densities (at -100 mV) measured in endolysosomal patch-clamp experiments as shown in Fig.1. Currents were elicited with PI(3,5)P₂ (1 μM). To test for statistical significance the one-way ANOVA test followed by Tukey's post-test was applied. ***, indicates p<0.001, **, indicates p<0.01. (B) Single capacitance values for the vesicles measured in the experiments presented in Fig.1.

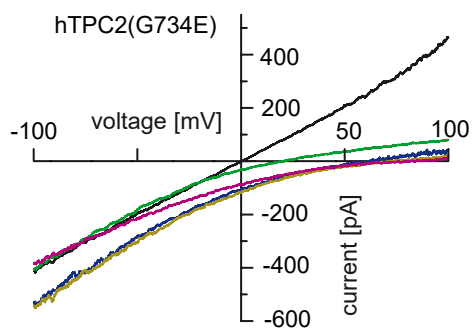
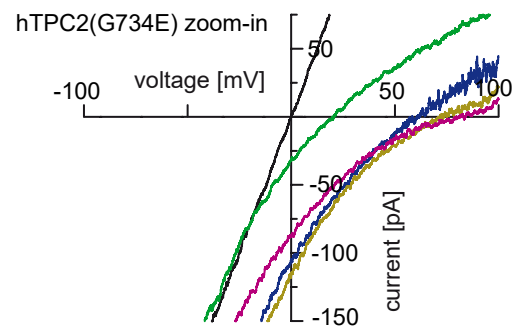
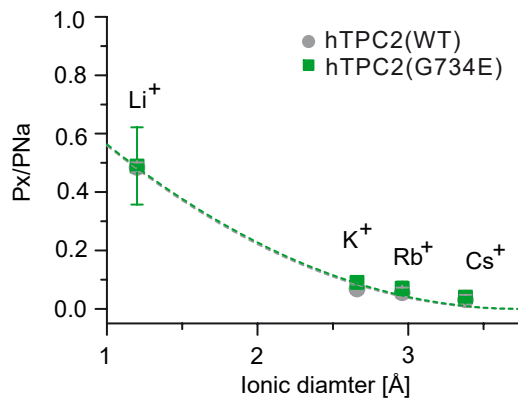


SI Figure 4

Effect of ATP on human TPC2 WT and G734E using the respective EC₈₀ values of PI(3,5)P₂ as activating concentrations or a fixed concentration of 1 μM. (A-B) Representative PI(3,5)P₂ (diC8) activated currents in vacuolin enlarged hTPC2 WT and hTPC2(G734E) expressing endolysosomal vesicles using the respective EC₈₀ values as activating PI(3,5)P₂ concentrations and different concentrations of ATP as indicated to block the currents. (C) ATP dose response curves from experiments as shown in A-B. (D-E) Similar experiments as in A-B using a fixed PI(3,5)P₂ concentration of 1 μM as activating concentration and different concentrations of ATP as indicated to block the currents. (F) ATP dose response curves from experiments as shown in D-E. In all experiments currents were elicited by applying 500-ms voltage ramps from -100 to +100 mV every 5 s. To test for statistical significance the Student's *t*-test, unpaired was applied. * indicates $p < 0.05$.

A**B**

Torin-1	-	+	-	-	+	-
Rapamycin	-	-	+	-	-	+

C**D****E**Luminal: 160 Na⁺

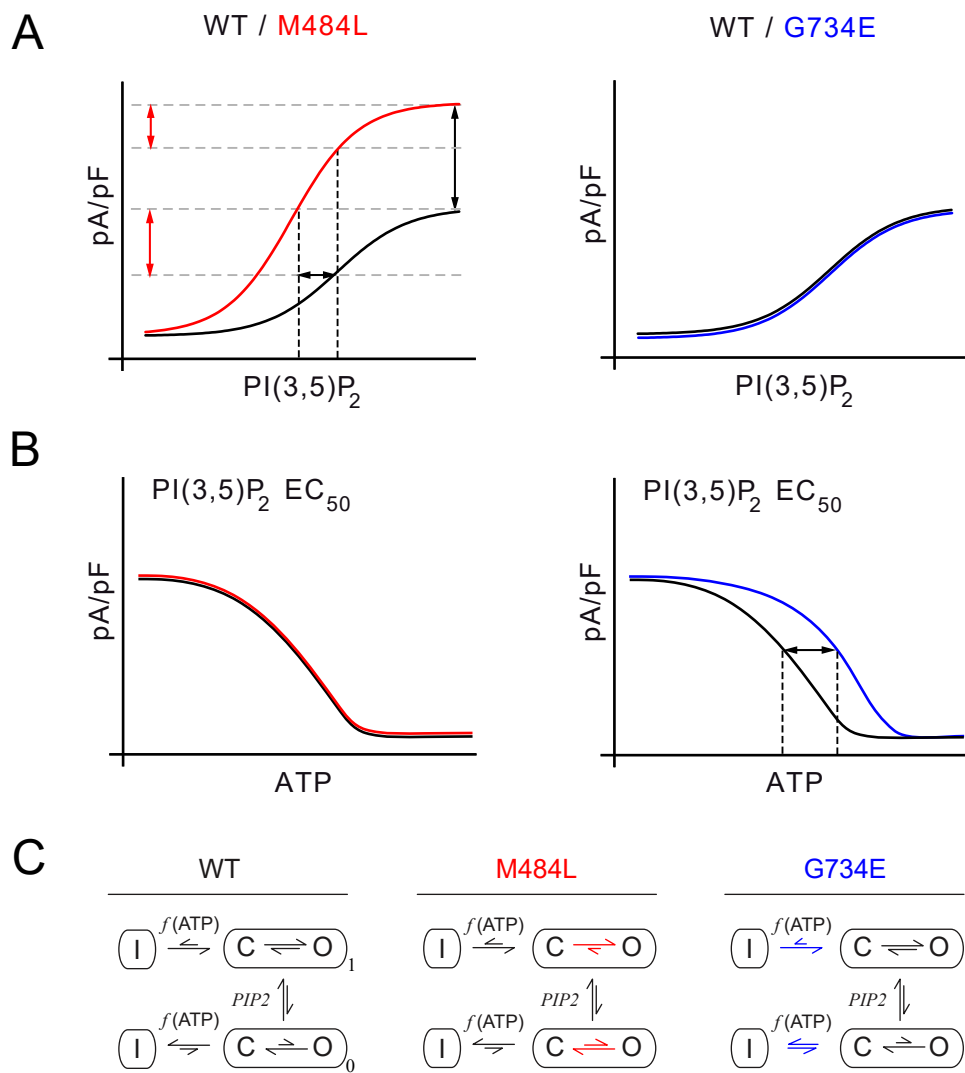
Cytoplasmic:

— 160 Na⁺— 160 Li⁺— 160 K⁺— 160 Rb⁺— 160 Cs⁺+ PI(3,5)P₂

SI Figure 5

Effect of mTOR inhibitors on M484L and ion substitution experiments for G734.

(A) Representative PI(3,5)P₂ (1 μM) activated currents in vacuolin enlarged hTPC2(M484L) expressing endolysosomal vesicles and the respective blocking effects of 2 μM torin-1 or 1 μM rapamycin. Cells were incubated with torin-1 for 12 hours or with rapamycin for 10 minutes before experimentation. Currents were measured in the absence of ATP. (B) Statistical summary of data as shown in A including respective basal currents. Shown are average current densities at -100 mV. (C) Endolysosomal patch-clamp experiments showing PI(3,5)P₂-activated hTPC2(G734E) currents under bi-ionic conditions with luminal Na⁺ and bath solutions containing the following monovalent cations, respectively: Li⁺, K⁺, Rb⁺ and Cs⁺. (D) Expanded view of C. (E) Summary of data as shown in C-D. Shown are the relative permeabilities (P_x/P_{Na}) of the different cations plotted against the diameter of cations. The dashed lines are fitted to Equation 2 (see method section for details).



SI Figure 6

Model for the different channel properties in TPC2 variants. (A) Shown are schematic PI(3,5)P₂ dose-response curves (DRCs) of WT versus M484L (A, left) and WT versus G734E (A, right). (B) Schematic ATP DRCs of WT versus M484L (B, left) and WT versus G734E (B, right) using the respective EC₅₀ concentrations of PI(3,5)P₂ to activate. Compared to WT the DRC for PI(3,5)P₂ is changed in the M484L variant while the ATP inhibition curve is not. The opposite effect can be seen when comparing WT with the G734E variant: Compared to WT the DRC for PI(3,5)P₂ is unchanged in the G734E variant while the ATP inhibition curve is changed. Therefore, the overall system response is determined by the difference in DRC for PI(3,5)P₂ in the M484L variant while it is determined by the ATP inhibition curve in the G734E variant. Gain of function in the M484L variant is evident by the increased maximal PI(3,5)P₂ activation current density (increased efficacy) and by the lower EC₅₀ for PI(3,5)P₂ (increased potency) compared to WT (A). At a fixed ATP concentration one would expect the same fractional block in WT and the M484L variant (inhibition curve is identical; B, left). However, this fractional block is determined by the DRC for PI(3,5)P₂ and depends on the PI(3,5)P₂ concentration. Inhibition of mTOR which likely mediates the ATP effect on TPC2 would revert the block and increase current density in both channel variants. The fractional increase would likewise be determined by the DRC for PI(3,5)P₂ and depend on the PI(3,5)P₂ concentration. The dashed grey lines and red double arrows (A, left) indicate the range for further increase in channel activity at the EC₅₀ of WT. At this concentration M484L has almost reached its activation plateau. If the activating PI(3,5)P₂ concentration is at the EC₅₀ of WT, then mTOR inhibition would result in a smaller increase in activity in M484L compared to WT. (A, right) In WT and G734E the DRC and EC₅₀ values for PI(3,5)P₂ are similar. By contrast, the ATP inhibition curve is shifted to higher ATP concentrations in G734E (B, right). Thus, at the same ATP concentration (= activation of mTOR) WT would be blocked more efficiently than G734E. Inhibition of mTOR would increase channel activity in both WT and G734E. However, at the same PI(3,5)P₂ concentration (see Fig. 3) the increase in activity would be expected to be stronger in G734E than in WT. (C) Model of the effects shown in A and B (C = closed, I = inactive, O = open). Left panel (WT): In the absence of PI(3,5)P₂, the channels can open but the openings are very rare. This is indicated by the equilibrium constant biased toward the closed state. Upon binding to PI(3,5)P₂, the channels can open much better as the equilibrium is biased towards the open state. Thus, addition of PI(3,5)P₂ will increase the currents substantially. Inactivation: ATP binding to mTOR triggers channel inactivation, possibly via a two-step process. First activated mTOR binds to an effector interface, and then that triggers a conformational change that manifests as inactivation. Moreover, channels unbound to PI(3,5)P₂ will preferentially enter the inactivated state. Center panel (M484L): C1 to O1 and C0 to O0 are enhanced as a result of the pore-dilation. Right panel (G734E): Activation process is not affected but the ATP sensitivity is reduced with no effect on the activation.